DOI: 10.1002/ejic.200600636

Coordination Chemistry of 3-Mercapto-2-(mercaptomethyl)propanoic Acid (Dihydroasparagusic Acid) with Iron and Nickel

Phillip I. Volkers,[a] Thomas B. Rauchfuss,*[a] and Scott R. Wilson[a]

Keywords: Iron / Nickel / S ligands / Bridging ligands / Coordination modes

The first transition-metal complexes bearing the natural product dihydroasparagusic acid, $(HSCH_2)_2CHCO_2H$, as a ligand are reported. Various coordination modes and nuclearities are demonstrated for the chelating ligand by a series of iron and nickel complexes. $Fe_2[(SCH_2)_2CHCO_2H](CO)_6$ retains carbonyl substitution reactivity typical of $Fe_2(SR)_2(CO)_6$ complexes, yet carboxy coordination to Fe^I was unobserved. Coupling of the carboxylic acid with amines yields the corresponding amides $Fe_2[(SCH_2)_2CHC(O)NHR](CO)_6$ (R = Et, gly–*O*–*t*Bu). $Fe_2[(SCH_2)_2CHCO_2H](CO)_4(PMe_3)_2$ catalyzes H_2 production, but no better than unfunctionalized alkyl dithiolate analogs. Reactions of the ligand with $NiCl_2$(dppe) afforded mono-, di-, and trinuclear complexes. Noteworthy is $Ni_3[(SCH_2)_2CHCO_2]_2(dppe)_2$, which features an octahedrally coordinated Ni^{II} center linked to a pair of square-planar Ni^{II} centers.

Introduction

The coordination properties of the natural product dihydroasparagusic acid,[1] $(HSCH_2)_2CHCO_2H$, has received little attention.[2] This compound has long been known, is prepared easily, and offers the possibility of serving as a functionalized bridging dithiolate ligand.[3,4] Our interest in exploring its coordination properties was motivated by the occurrence of propanedithiolate or the isosteric 2-azapropane-1,3-dithiolate as a cofactor in the iron hydrogenases.[5–7]

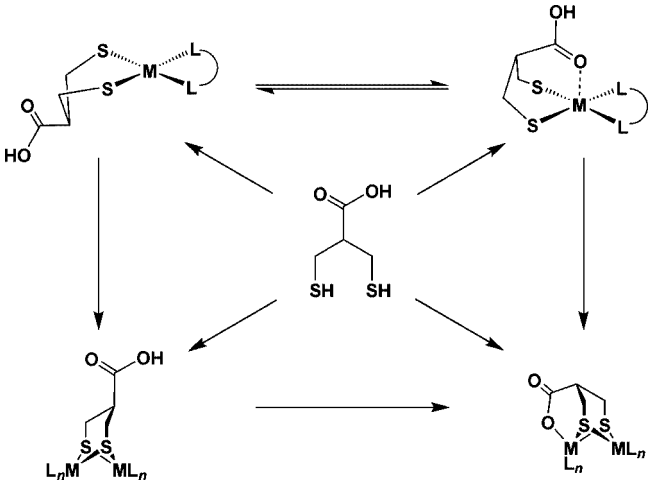

Scheme 1. General coordination modes for $(HSCH_2)_2CHCO_2H$.

In considering the coordinating properties of asparagusic acid, one can anticipate several motifs: *S*,*S*-bidentate; *S*,*S*,*O*-tridentate; and dinuclear derivatives of each of these (Scheme 1). Examples of such coordination modes are presented here using iron and nickel platforms. We were particularly interested in the possibility that the carboxylic acid functionality in $Fe_2[(SCH_2)_2CHCO_2H](CO)_{6-x}L_x$ would permit attachment of functionality, affect electrocatalytic H_2 production,[8,9] or lead to more robust linkages between metal atoms.

Results and Discussion

I. Complexes with Iron

$Fe_2[(SCH_2)_2CHCOOH](CO)_6$

The air-stable parent complex, hereafter Fe_2(aspH)$(CO)_6$, was synthesized in 43% yield by the reaction of $Fe_3(CO)_{12}$ and dihydroasparagusic acid, $(HSCH_2)_2$CHCOOH ($aspH_3$). The preparation was more conveniently conducted in the presence of NEt_iPr_2, followed by acidification to produce Fe_2(aspH)$(CO)_6$. Crystallographic characterization of Fe_2(aspH)$(CO)_6$ verified the anticipated $Fe_2(SR)_2(CO)_6$ core and demonstrated hydrogen-bonding interactions between pairs of carboxyl groups (Figure 1, Table 1). The carboxylic acid occupies an equatorial position on the cyclohexane-like FeS_2C_3 ring, projecting orthogonally with respect to the Fe–Fe vector.

Fe_2(aspH)$(CO)_6$ undergoes the transformations expected for a carboxylic acid (Scheme 2). Amide-bond formation with $EtNH_2$ was effected using a phosphonium-based coup-

[a] Department of Chemistry, University of Illinois, 601 S. Goodwin Ave., Urbana, IL 61801, USA

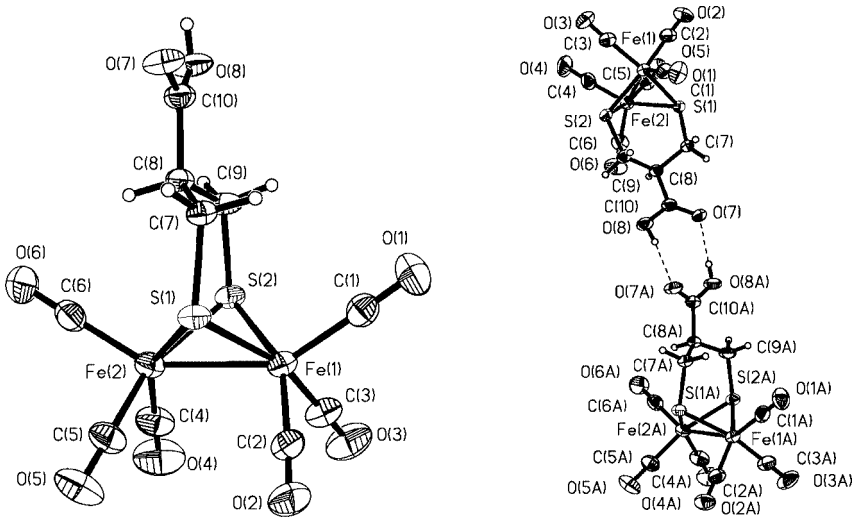

Figure 1. Left: structure of $Fe_2(aspH)(CO)_6$ with thermal ellipsoids set at the 50% probability level. Right: structure of the hydrogen-bonded dimer of $Fe_2(aspH)(CO)_6$. Selected distances [Å] and angles [°]: Fe(1)–Fe(2) 2.5130(8), Fe(1)–C(1) 1.813(2), Fe(1)–C(2) 1.803(2), Fe(1)–C(3) 1.811(2), Fe(1)–S(1) 2.2485(8), Fe(1)–S(2) 2.2535(7), Fe(2)–C(4) 1.794(2), Fe(2)–C(5) 1.797(2), Fe(2)–C(6) 1.808(2), Fe(2)–S(2) 2.2529(7), Fe(2)–S(1) 2.2554(7), O(7)–C(10) 1.216(2), O(8)–C(10) 1.314(2); S(1)–Fe(1)–S(2) 85.21(3), S(2)–Fe(2)–S(1) 85.06(3).

Table 1. Selected crystallographic data for iron-containing asparagusic complexes.

	$Fe_2(aspH)(CO)_6$	$Fe_2[(SCH_2)_2CHCONHEt](CO)_6$	$Fe_2[(SCH_2)_2CHCONHCH_2CO_2tBu](CO)_6$
Empirical formula	$C_{10}H_6Fe_2O_8S_2$	$C_{12}H_{11}Fe_2NO_7S_2$	$C_{16}H_{17}Fe_2NO_9S_2$
Formula mass	429.97	457.04	543.13
T [K]	193(2)	193(2)	193(2)
λ [Å]	0.71073	0.71073	0.71073
Crystal system	monoclinic	monoclinic	monoclinic
Space group	$C2/c$	$P2_1/c$	$P2_1/c$
a [Å]	23.521(8)	14.267(3)	11.623(2)
b [Å]	9.672(3)	13.792(3)	16.309(3)
c [Å]	14.383(5)	9.307(2)	24.543(4)
α [°]	90	90	90
β [°]	113.389(5)	106.954(4)	95.558(3)
γ [°]	90	90	90
V [Å^3]	3003.3(17)	1751.8(7)	4630.2(14)
Z	8	4	8
ρ (calcd.) [g/cm^3]	1.902	1.733	1.558
μ (Mo-K_α) [mm^{-1}]	2.244	1.926	1.477
F(000)	1712	920	2208
Crystal size [mm]	$0.44 \times 0.40 \times 0.16$	$0.44 \times 0.09 \times 0.05$	$0.34 \times 0.26 \times 0.20$
θ range [°]	1.89–28.27	2.10–28.31	1.76–25.38
Reflections collected	14606	17196	36784
Independent reflections	3668 [R(int) = 0.0357]	4292 [R(int) = 0.0671]	8492 [R(int) = 0.0573]
Absorption correction	integration	integration	integration
Max./min. transmission	0.7170/0.4373	0.9099/0.4495	0.7641/0.6190
Goodness-of-fit on F^2	1.03	0.875	0.918
Final R indices [$I > 2\sigma(I)$]	R_1 = 0.0274	R_1 = 0.0368	R_1 = 0.0330
	wR_2 = 0.0665	wR_2 = 0.0646	wR_2 = 0.0643
R indices (all data)	R_1 = 0.0389	R_1 = 0.0844	R_1 = 0.0651
	wR_2 = 0.0709	wR_2 = 0.0727	wR_2 = 0.0716
Largest diff. peak/hole [e·Å^{-3}]	0.308/–0.365	0.533/–0.322	0.321/–0.240

ling agent. The crystallographic characterization of $Fe_2[(SCH_2)_2CHCONHEt](CO)_6$ confirms the structure (Figure 2, Table 1). The amide substituent is again equatorial with respect to the cyclohexane-like FeS_2C_3 ring and the nitrogen is planar. The occurrence of two identical splitting patterns in the ^{1}H NMR spectrum is attributed to *cisoid* and *transoid* rotamers of the amide, consistent with restricted rotation about the C(O)–N bond. Coupling of $Fe_2(aspH)(CO)_6$ with glycine *tert*-butyl ester afforded the corresponding amido ester $Fe_2[(SCH_2)_2CHCONHCH_2CO_2tBu](CO)_6$, which exhibited crystallographic features akin to those in the ethyl derivative (Figure 3, Table 1). Again, two rotamers were observed in the ^{1}H NMR spectrum.

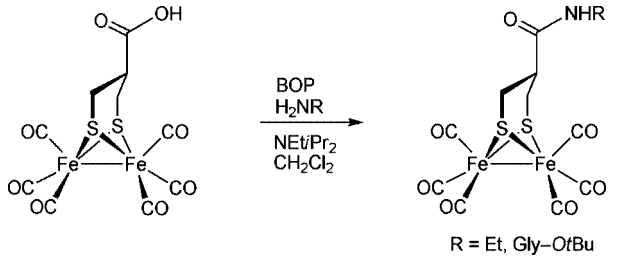

Scheme 2. Synthetic route for amide-bond derivatization of $Fe_2(aspH)(CO)_6$.

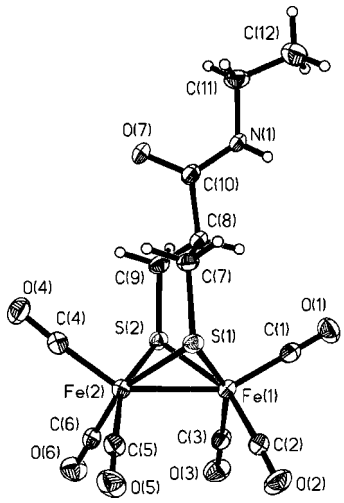

Figure 2. Structure of $Fe_2[(SCH_2)_2CHCONHEt](CO)_6$ with thermal ellipsoids set at the 50% probability level. Selected distances [Å] and angles [°]: Fe(1)–Fe(2) 2.5167(8), Fe(1)–C(1) 1.800(3), Fe(1)–C(2) 1.797(3), Fe(1)–C(3) 1.801(3), Fe(1)–S(1) 2.2542(9), Fe(1)–S(2) 2.2574(8), Fe(2)–C(4) 1.795(3), Fe(2)–C(5) 1.799(3), Fe(2)–C(6) 1.807(3), Fe(2)–S(1) 2.2497(9), Fe(2)–S(2) 2.2522(9); S(1)–Fe(1)–S(2) 85.07(3), S(1)–Fe(2)–S(2) 85.30(3).

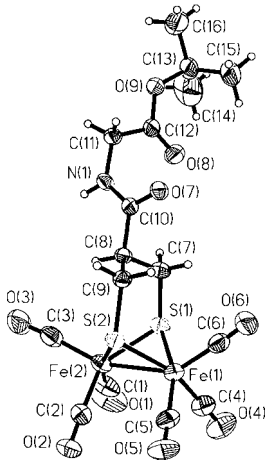

Figure 3. Structure of $Fe_2[(SCH_2)_2CHCONHCH_2CO_2tBu](CO)_6$ with thermal ellipsoids set at the 50% probability level. Selected distances [Å] and angles [°]: Fe(1)–Fe(2) 2.5141(7), C(1)–Fe(2) 1.791(3), C(2)–Fe(2) 1.795(3), C(3)–Fe(2) 1.806(4), C(4)–Fe(1) 1.801(3), C(5)–Fe(1) 1.798(3), C(6)–Fe(1) 1.797(3), S(1)–Fe(1) 2.2567(8), S(1)–Fe(2) 2.2574(9), S(2)–Fe(1) 2.2532(8), S(2)–Fe(2) 2.2676(8); S(2)–Fe(1)–S(1) 85.32(3), S(1)–Fe(2)–S(2) 84.96(3).

Acid-Base Properties

Although only poorly soluble in MeOH, $Fe_2(aspH)(CO)_6$ was found to dissolve upon addition of Et_3N, indicative of the formation of $Et_3NH[Fe_2(asp)(CO)_6]$. The ν_{CO} region in the solution IR spectrum of this deprotonated compound exhibited negligible shifts relative to $Fe_2(aspH)(CO)_6$, indicating minor electronic influence of the pendant carboxy/carboxylate group on the diiron unit. The easy deprotonation of $Fe_2(aspH)(CO)_6$ interfered with experiments aimed at its decarbonylation using Me_3NO.[10] Rather than the usual red-to-purple color change observed upon decarbonylation of $Fe_2(SR)_2(CO)_6$,[9] solutions deposited a brown precipitate, presumably of $Me_3NOH[Fe_2(asp)(CO)_6]$.

Substitution Reactions of $Fe_2(aspH)(CO)_6$

Upon heating in the presence of excess PMe_3, $HNEtiPr_2[Fe_2(asp)(CO)_6]$ converted readily into $HNEtiPr_2[Fe_2(asp)(CO)_4(PMe_3)_2]$. The ^{31}P NMR spectrum of the product showed two equally intense singlets, indicating the nonequivalency imposed by the pendant carboxylate group. IR measurements in the ν_{CO} region indicate that this salt is very similar electronically to related derivatives, e.g. $Fe_2(S_2C_3H_6)(CO)_4(PMe_3)_2$.[11]

Substitution of the CO ligands in $Fe_2(aspH)(CO)_6$ by cyanide was also explored. IR spectroscopic measurements in the ν_{CO} region established that the first equivalent of CN^- deprotonated the carboxylic acid. The prevalence of monosubstituted product, $[Fe_2(asp)(CN)(CO)_5]^{2-}$ ($\nu_{CN,CO}$ = 2091, 2028, 1974, 1952, 1914), shows that the pendant carboxylate group inhibits a second cyanide ion from attacking the unsubstituted iron center. When the carboxylic acid was first deprotonated with an amine base, followed by treatment with 1 equiv. of CN^-, we again obtained the monosubstituted product. Upon heating in the presence of an additional equivalent of CN^-, $[Fe_2(asp)(CN)(CO)_5]^{2-}$ converted into the dicyanide derivative, $[Fe_2(asp)(CN)_2(CO)_4]^{3-}$, as established by IR spectroscopy ($\nu_{CN,CO}$ = 2074, 1960, 1919, 1880).

Electrochemical Studies

Cyclic voltammetry studies showed that MeCN solutions of $Fe_2(aspH)(CO)_6$ reduce at –1.20 and –1.96 V vs. Ag/AgCl, corresponding to Fe^IFe^I/Fe^0Fe^I and Fe^0Fe^I/Fe^0Fe^0 couples, respectively.[12] Addition of 1–4 equiv. of HOAc caused an increase in the cathodic current at ca. –1.8 V, characteristic of catalytic H_2 production.[12] The electrocatalytic properties do not, however, differ significantly from analogous $Fe_2(S_2C_3H_6)(CO)_6$. In a confirmatory experiment, a 1:1 mixture of $Fe_2(aspH)(CO)_6$ and $Fe_2(S_2C_3H_6)(CO)_6$ in acetonitrile was analyzed electrochemically. The mixture displayed reduction events at –1.20 and –1.96 V, indicating that the two compounds had overlapping reduction events. Similarly, electrochemical analyses of $Fe_2(aspH)(CO)_4(PMe_3)_2$ and HOAc or HOTs showed catalytic H_2 production at –1.86 or –1.21 V, respectively, typical of $Fe_2(S_2C_xH_{2x})(CO)_4(PMe_3)_2$ species.[12,13]

II. Complexes with Nickel

Ni(aspH)(dppe)

Treatment of $NiCl_2$(dppe) with a solution of $aspH_3$ and base yielded orange mononuclear Ni(aspH)(dppe) (Scheme 3).[14,15] The crystallographic characterization of Ni(aspH)(dppe) confirmed the expected square-planar coordination and intermolecular hydrogen bonding (Figure 4, Table 2). The six-membered chelate ring adopts a twist-boat conformation, which projects the carboxylic acid away from the metal center. Ni(aspH)(dppe) was only slightly soluble in MeOH; however, the salt resulting from treatment of Ni(aspH)(dppe) with NEt_3 was found to dissolve in both MeOH and CH_2Cl_2.

$[Ni_2(aspH)(dppe)_2]^{2+}$ and $Ni_3(asp)_2(dppe)_2$

These di- and trinuclear species[16] were initially obtained as byproducts of the synthesis of Ni(aspH)(dppe). $[Ni_2(aspH)(dppe)_2]Cl_2$ (Scheme 3) was identified by ESI-MS, and its ^{31}P NMR spectrum displays two doublets. Isolation of the dinuclear dication was attempted by forming its BPh_4^- salt. Surprisingly, the ^{31}P NMR spectrum displays only one, albeit broad, resonance for the inequivalent phosphane ligands. The dinuclear product was identified again by ESI-MS and a preliminary X-ray crystallographic analysis as its BPh_4^- salt. The salt was unstable as a solid under N_2.

Upon standing, solutions of Ni(aspH)(dppe) and $[Ni_2(aspH)(dppe)_2](Cl)_2$ deposited crystals of the trinuclear spe-

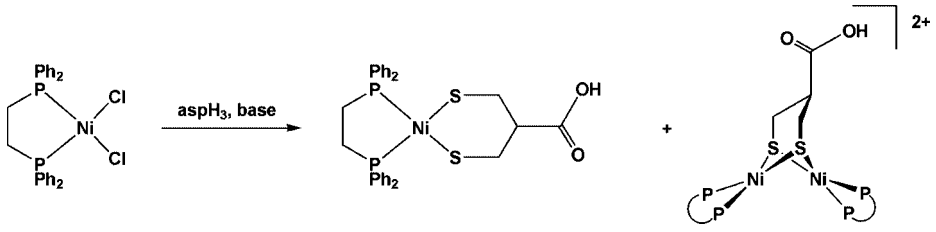

Scheme 3. Synthetic route to Ni(aspH)(dppe) and $[Ni_2(aspH)(dppe)_2]^{2+}$.

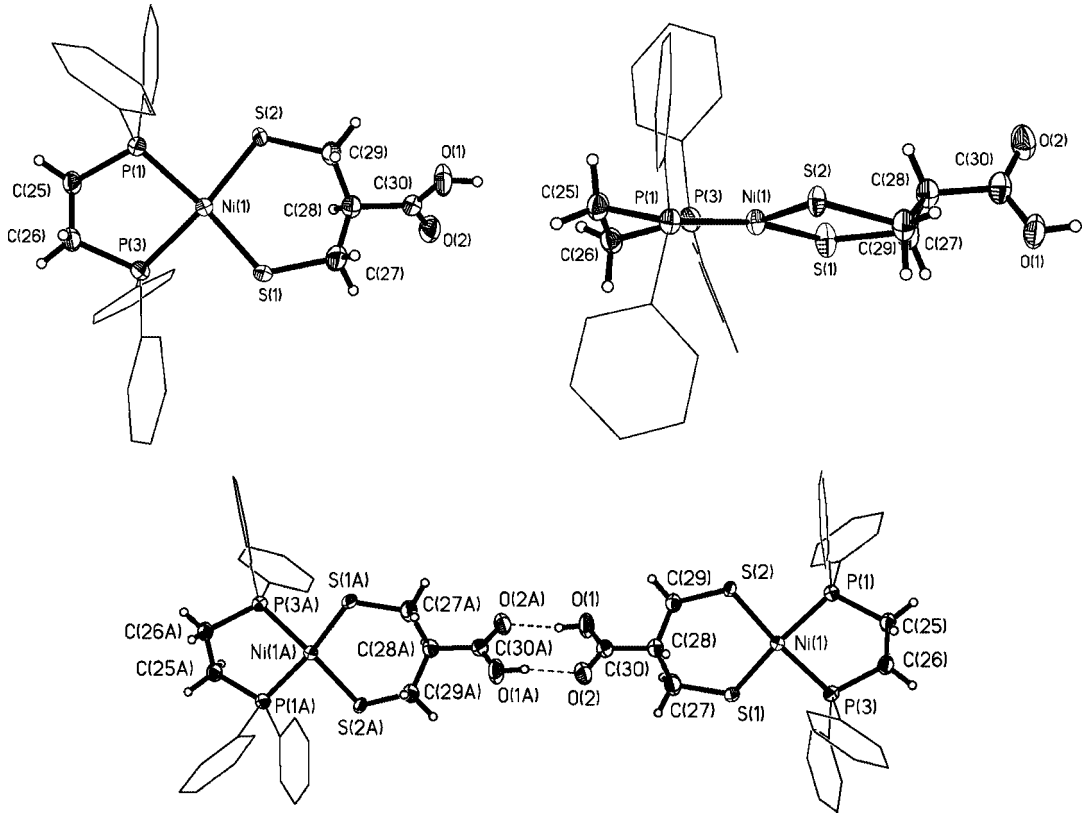

Figure 4. Top left: structure of Ni(aspH)(dppe) with thermal ellipsoids set at the 50% probability level. Top right: orthogonal view of Ni(aspH)(dppe). Bottom: structure of the hydrogen-bonded dimer of Ni(aspH)(dppe). Phenyl ellipsoids and phenyl hydrogen atoms are omitted for clarity. Selected distances [Å] and angles [°]: S(1)–Ni(1) 2.149(5), S(2)–Ni(1) 2.197(4), P(1)–Ni(1) 2.1772(6), P(3)–Ni(1) 2.1743(6); S(1)–Ni(1)–P(3) 87.76(10), S(1)–Ni(1)–P(1) 168.17(14), P(3)–Ni(1)–P(1) 86.51(2), S(1)–Ni(1)–S(2) 101.30(11), P(3)–Ni(1)–S(2) 165.84(11), P(1)–Ni(1)–S(2) 86.40(9).

Table 2. Selected crystallographic data for nickel-containing asparagusic complexes.

	Ni(aspH)(dppe)	$Ni_3(asp)_2(dppe)_2$
Empirical formula	$C_{30}H_{30}NiO_2P_2S_2$	$C_{62}H_{61}NNi_3O_4P_4S_4$
Formula mass	607.31	1312.37
T [K]	193(2)	193(2)
λ [Å]	0.71073	0.71073
Crystal system	monoclinic	triclinic
Space group	$P2_1/n$	$P\bar{1}$
a [Å]	11.242(2)	10.6763(5)
b [Å]	14.418(3)	11.3329(6)
c [Å]	17.256(3)	12.3295(7)
α [°]	90	76.447(3)
β [°]	92.569(3)	85.874(2)
γ [°]	90	79.774(2)
V [Å^3]	2794.2(9)	1426.49(13)
Z	4	1
ρ (calcd.) [g/cm^3]	1.444	1.528
μ (Mo-K_α) [mm^{-1}]	0.985	1.288
F(000)	1264	680
Crystal size [mm]	$0.38 \times 0.33 \times 0.22$	$0.22 \times 0.14 \times 0.09$
θ range [°]	1.84–25.34	1.70–30.00
Reflections collected	20742	44467
Independent reflections	5113	8302
	[R(int) = 0.0275]	[R(int) = 0.0239]
Absorption correction	integration	integration
Max./min. transmission	0.8425/0.6397	0.8983/0.7746
Goodness-of-fit on F^2	1.044	1.039
Final R indices [$I > 2\sigma(I)$]	R_1 = 0.0289	R_1 = 0.0255
	wR_2 = 0.0685	wR_2 = 0.0649
R indices (all data)	R_1 = 0.0366	R_1 = 0.0324
	wR_2 = 0.0715	wR_2 = 0.0689
Largest diff. peak/hole [e·Å^{-3}]	0.277/–0.236	0.402/–0.307

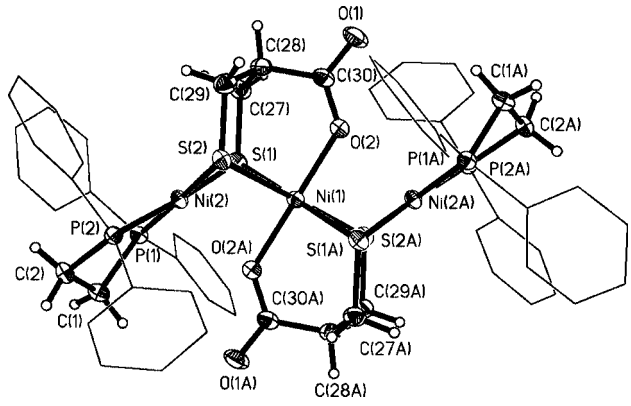

Figure 5. Structure of $Ni_3(asp)_2(dppe)_2$ with thermal ellipsoids set at the 50% probability level. The solvent molecules, phenyl ellipsoids, and phenyl hydrogen atoms are omitted for clarity. Selected distances [Å] and angles [°]: Ni(1)–O(2) 2.0172(15), Ni(1)–O(2A) 2.0172(15), Ni(1)–S(2A) 2.4424(5), Ni(1)–S(2) 2.4424(5), Ni(1)–S(1A) 2.4528(5), Ni(1)–S(1) 2.4528(5), Ni(1)–Ni(2A) 2.8423(3), Ni(2)–P(1) 2.1529(6), Ni(2)–P(2) 2.1670(6), Ni(2)–S(2) 2.2280(5), Ni(2)–S(1) 2.2350(6); O(2)–Ni(1)–O(2A) 180.0, O(2)–Ni(1)–S(2A) 89.43(5), O(2A)–Ni(1)–S(2A) 90.57(5), O(2)–Ni(1)–S(2) 90.57(5), O(2A)–Ni(1)–S(2) 89.43(5), S(2A)–Ni(1)–S(2) 180.000(19), O(2)–Ni(1)–S(1A) 87.98(4), O(2A)–Ni(1)–S(1A) 92.02(4), S(2A)–Ni(1)–S(1A) 81.724(17), S(2)–Ni(1)–S(1A) 98.276(17), O(2)–Ni(1)–S(1) 92.02(4), O(2A)–Ni(1)–S(1) 87.98(4), S(2A)–Ni(1)–S(1) 98.276(17), S(2)–Ni(1)–S(1) 81.724(17), S(1A)–Ni(1)–S(1) 180.0, O(2)–Ni(1)–Ni(2A) 58.05(4), O(2A)–Ni(1)–Ni(2A) 121.95(4), S(2A)–Ni(1)–Ni(2A) 49.158(13), S(2)–Ni(1)–Ni(2A) 130.842(13), S(1A)–Ni(1)–Ni(2A) 49.260(13), S(1)–Ni(1)–Ni(2A) 130.740(13), P(1)–Ni(2)–P(2) 87.32(2), P(1)–Ni(2)–S(2) 177.96(2), P(2)–Ni(2)–S(2) 90.71(2), P(1)–Ni(2)–S(1) 90.23(2), P(2)–Ni(2)–S(1) 175.79(2), S(2)–Ni(2)–S(1) 91.71(2), Ni(2)–S(1)–Ni(1) 74.514(11), Ni(2)–S(2)–Ni(1) 74.831(11).

cies analyzing as $Ni_3(asp)_2(dppe)_2$ (Scheme 4). The conversion was accelerated by exposure to air, and FD-MS of the resulting supernatant revealed formation of $dppeO_2$. Crystallographic analysis (Figure 5, Table 2) confirmed a trimetallic complex featuring an unusual Ni(μ-SR)$_2$Ni(μ-SR)$_2$Ni motif.[17–20] Unlike the well-precedented L_2Ni(μ-SR)$_2$Ni(μ-SR)$_2$NiL$_2$ motif, the central nickel atom in $Ni_3(asp)_2(dppe)_2$ is octahedral, being bound also to the two carboxylate ligands with Ni–O distances of 2.0 Å (Figure 5). The terminal nickel centers are square-planar and low-spin. The terminal Ni^{II} centers are more tightly bonded to the sulfur atoms (2.22–2.23 Å), whereas the interior nickel center exhibits longer bonds to the sulfur atoms (2.44–2.45 Å), reflecting its higher coordination number. Insolubility of the crystals precluded further analysis of, and reactivity experiments on, the trinuclear species.

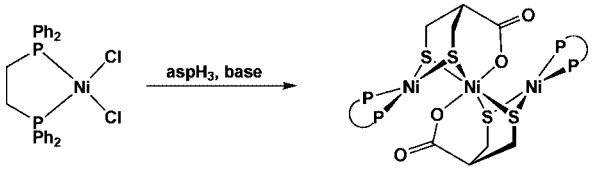

Scheme 4. Synthetic route to $Ni_3(asp)_2(dppe)_2$.

Summary

The first transition-metal complexes bearing the chelating ligand asparagusic acid are reported. Electronically, the pendant carboxyl group does not perturb the *S*,*S* coordination to metal centers, as evidenced by IR and CV studies. The ligand enables straightforward derivatization to be performed on the pendant carboxyl group. Substitution chemistry at the metal centers is also retained, but in the case of $Fe_2(aspH)(CO)_6$ the reactions are slower than the related propanedithiolate complex. In general, the bulk of the dithiolate backbone strongly influences the rates of substitution at the underlying $Fe(CO)_3$ units. The dithiolate–carboxylate can serve as a bridging tridentate chelate by binding a pair of metal centers through *S*,*S*,*O* ligation.

Pickett, Darensbourg, and our group have demonstrated the utility of pendant coordinating groups in modeling the active site of the Fe H_2-ases.[21–23] Such pendant ligands, however, were always soft, being phosphanes, thioethers, or alkenes. In the case of $Fe_2(aspH)(CO)_6$ or its amides, we observed no evidence of coordination of the hard oxygen ligands to Fe^{I}. Furthermore, we observed no indication that the carboxylic acid or its anion usefully influence the catalytic chemistry of the related $Fe_2(aspH)(CO)_4(PMe_3)_2$ complexes. This lack of an effect is consistent with a mechanism whereby catalysis is localized on the region between the two iron centers.

Experimental Section

General: Nylon syringe filters (0.2 μm) were acquired from Nalgene. (Benzotriazol-1-yloxy)tris(dimethylamino)phosphonium hexafluorophosphate (BOP) was acquired from ChemImpex Intl. All other chemicals were acquired from Aldrich and used without further purification. Solvents were dried by distillation or were dispensed through two 1-m columns of activated alumina. Solvents were further purified by degassing with a nitrogen purge. Reactions were performed under purified nitrogen using either standard Schlenk techniques or a glove box.

Dihydroasparagusic Acid [3-Mercapto-2-(mercaptomethyl)propanoic Acid]: The free ligand was prepared based on the method of Singh and Whitesides.[4] After concentrating the EtOAc extract, the dithiol was extracted into hexane and subsequent slow evaporation of solvent yielded white crystals in 54% yield based on 2-(bromomethyl)propenoic acid.

$Fe_2(aspH)(CO)_6$: NEt*i*Pr$_2$ (921 μL, 5.29 mmol) was added to a THF solution (20 mL) of 3-mercapto-2-(mercaptomethyl)propanoic acid (805 mg, 5.29 mmol). An additional 45 mL of THF was added followed by $Fe_3(CO)_{12}$ (2.421 g, 4.81 mmol). Gas evolution commenced immediately, and the color of the solution changed from green-black to yellow-red, concomitant with the formation of a yellow precipitate. The mixture was refluxed for 2.25 h. The resulting dark red solution was filtered in air through a pad of Celite; removal of the solvent gave a red oil. The product was extracted into MeOH, and this extract was filtered again through Celite and concentrated in vacuo. The residue was taken up in 15 mL of CH_2Cl_2, treated with trifluoroacetic acid (600 μL, 8.08 mmol), and chromatographed on silica gel, eluting with MeCN/CH_2Cl_2 (1:7, v:v). The second red band was collected and concentrated in vacuo to give a red crystalline product. Yield: 888 mg (43%). $C_{10}H_6Fe_2O_8S_2$ (429.98): calcd. C 27.93, H 1.41; found C 27.79, H 1.13. ^{1}H NMR (500 MHz, CD_3OD): δ = 2.92 (dd, 2 H, SC*H*H), 2.16 (br., 1 H, C*H*COO), 1.81 (dd, 2 H, SCH*H*) ppm. The solid product decomposed at 118 °C. IR (MeOH): ν_{CO} = 2076 (vs), 2037 (vs), 1997 (vs), 1730 (m, monomer), 1710 (m, dimer) cm^{-1}. FD-MS: *m*/*z* = 429.8 [M$^+$], 373.8 [M$^+$ – 2 CO].

Alternative Synthesis of $Fe_2(aspH)(CO)_6$: A mixture of $Fe_3(CO)_{12}$ (5.00 g, 9.92 mmol) and 3-mercapto-2-(mercaptomethyl)propanoic acid (1.51 g, 9.92 mmol) in toluene (100 mL) was heated at 80 °C for 30 min, resulting in a red solution and a fine orange precipitate. The cooled reaction mixture was filtered through a pad of Celite, and the filtrate was concentrated to dryness. The product was extracted with MeCN and was filtered through a nylon membrane (0.2 μm). The solvent was removed to afford a red powder. Single crystals were grown by cooling a concentrated CH_2Cl_2 solution to –20 °C. Yield: 1.55 g (36%).

$Fe_2[(SCH_2)_2CHC(O)NHEt](CO)_6$: (Benzotriazol-1-yloxy)tris(dimethylamino)phosphonium hexafluorophosphate (103 mg, 0.233 mmol) was added to a solution of $Fe_2(aspH)(CO)_6$ (100 mg, 0.233 mmol) in $CHCl_3$ (5 mL) followed by H_2Net (17 μL, 0.2114 mmol). After stirring for 2 min, the coupling reaction was initiated upon addition of NEt*i*Pr$_2$ (55 μL, 0.317 mmol). The reaction was monitored by TLC. After 21 h, the reaction solution was concentrated in vacuo before being chromatographed on silica gel, eluting with MeOH/CH_2Cl_2 (5:95, v:v). The first red band was collected, and solvent removal by rotary evaporation yielded an orange powder. Single crystals were grown from a MeOH solution that was cooled to –20 °C. Yield: 30 mg (31%). $C_{12}H_{11}Fe_2NO_7S_2$ (457.05): calcd. C 31.54, H 2.43, N 3.06; found C 32.76, H 2.51, N 3.37. ^{1}H NMR (400 MHz, $CDCl_3$): δ = 3.21 (dq, 2 H, NCH_2), 2.66 (dd, 2 H, SCH_a), 1.85 [m, 3 H, SCH_b and $(SCH_2)_2$C*H*], 1.11 (t, 3 H, NCH$_2$CH_3) ppm. IR (MeOH): ν_{CO} = 2076 (vs), 2037 (vs), 1997 (vs), 1660 [m, C(O)N], 1563 (w, C–N stretch coupled to N–H deformation), 1310 (w, C–N) cm^{-1}. FD-MS: *m*/*z* = 456.9 (100) [M$^+$], 428.9 (23) [M$^+$ – CO], 400.8 (80%, M$^+$ – 2 CO).

$Fe_2[(SCH_2)_2CHCONHCH_2CO_2tBu](CO)_6$: [BOP]$PF_6$ (123 mg, 0.279 mmol) was added to a solution of $Fe_2(aspH)(CO)_6$ (120 mg, 0.279 mmol) in CH_2Cl_2 (5 mL) followed by the addition of Gly–*Ot*Bu·HCl (42 mg, 0.211 mmol). Addition of NEt*i*Pr$_2$ (110 μL, 0.63 mmol) and stirring for 2 h produced a clear, dark red solution. A concentrated CH_2Cl_2 solution was chromatographed on silica gel, eluting with MeOH/CH_2Cl_2 (5:95, v:v). Evaporation of solvent from the first red-orange band yielded a red-orange solid. Single crystals were grown by layering a CH_2Cl_2 solution of the compound with hexane followed by cooling to –20 °C. Yield: 38 mg (28%). $C_{16}H_{17}Fe_2NO_9S_2$ (543.14): calcd. C 35.38, H 3.15, N 2.58; found C 35.31, H 3.18, N 2.89. ^{1}H NMR (500 MHz, $CDCl_3$): δ = 5.81 (t, 1 H, N*H*), 3.84 (d, 2 H, NCH_2), 2.71 (dd, 2 H, SCH*H*), 1.91 (m, 3 H, SC*H*H and C*H*CO), 1.46 [s, 9 H, C(CH_3)$_3$] ppm. IR (MeOH): ν_{CO} = 2075 (m), 2036 (vs), 1997 (s), 1748 [w, C(O)-OCMe$_3$], 1668 [w, NC(O), amide I]; 1558 (w, C–N and N–H, amide II) cm^{-1}. FD-MS: *m*/*z* = 542.9 [M$^+$], 487 [M$^+$ – 2 CO].

Ni(aspH)(dppe): NaOMe (2 equiv.) in MeOH (40 mL) was added to a mixture of $NiCl_2$(dppe) (835 mg, 1.58 mmol) and aspH_3 (240 mg, 1.58 mmol) in MeOH (40 mL). The immediately resulting dark red solution yielded a bright orange precipitate after 1 h. After 4 h, volatiles were removed in vacuo. The residue was washed with 3 × 5 mL of MeOH to remove $[Ni_2(\mu,\mu'\text{-aspH})(dppe)_2]^{2+}$ and other impurities, leaving a bright orange powder. Yield: 577 mg (60%). Single crystals were grown by layering a CH_2Cl_2 solution of the compound with Et_2O. $C_{30}H_{30}NiO_2P_2S_2$ (607.34): calcd. C 59.33, H 4.98; found C 59.06, H 4.93. ^{1}H NMR (500 MHz, $CDCl_3$): δ = 10.30 (br. s, 1 H, COO*H*), 7.83–7.79 and 7.55–7.46 (m, 20 H, PC$_6H_5$), 3.10 [quint, 1 H, $(SCH_2)_2$C*H*], 2.79–2.64 (m, 4 H, SCH_2), 2.18 (d, 4 H, PCH_2) ppm. ^{31}P NMR (202 MHz, $CDCl_3$): δ = 57.92 (s). FD-MS: *m*/*z* = 606.1 [M$^+$ – H], 398 [dppe].

$[Ni_2(aspH)(dppe)_2](X)_2$ (X = Cl$^-$, BPh_4^-): NaOMe (2 equiv.) in MeOH (5 mL) was added to a mixture of $NiCl_2$(dppe) (200 mg, 0.379 mmol) and aspH_3 (58 mg, 0.379 mmol) in MeOH (5 mL). The solvent was removed in vacuo from the resulting clear, dark red solution after 5.5 h. ^{31}P NMR (202 MHz, CD_3CN): δ = 59.889 [s, 1 P, $NiCl_2$(dppe)], 57.738 [s, 1 P, Ni(aspH)(dppe)], 53.149 and 53.028 (d, 9 P, $[Ni_2(aspH)(dppe)_2]^{2+}$), 50.470 and 50.349 (d, 9 P, $[Ni_2(aspH)(dppe)_2]^{2+}$) ppm. ESI-MS: *m*/*z* (%) = 1099.4 (100) [{$[Ni_2(aspH)(dppe)_2]Cl$}$^+$], 1063.1 (2) $[Ni_2(asp)(dppe)_2]^+$, 532.3 (12) $[Ni_2(aspH)(dppe)_2]^{2+}$. The product was extracted into 5 mL of MeOH, filtered through a pad of Celite, and treated with a solution of $NaBPh_4$ (140 mg, 0.40791 mmol) in MeOH (3 mL). The resulting yellow-orange precipitate was washed with 15 mL MeOH and dried in vacuo. Yield: 173 mg (27%). Single crystals were grown from an acetone solution layered with methanol. ^{31}P NMR (202 MHz, CD_3CN): δ = 57.46 (br. s) ppm. ESI-MS: *m*/*z* (%) = 1063.3 (10) $[Ni_2(asp)(dppe)_2]^+$, 532.0 (100) $[Ni_2(aspH)(dppe)_2]^{2+}$.

$Ni_3(asp)_2(dppe)_2$: A mixture of $NiCl_2$(dppe) (100 mg, 0.18939 mmol) and aspH_3 (28.8 mg, 0.18939 mmol) in MeCN (15 mL) in air was treated with NEt_3 (79.2 μL, 0.56817 mmol). Upon standing for 3 h, a crystalline black precipitate began forming. After 1 d, the supernatant was decanted. The extremely dark maroon crystalline solid was collected and dried in air. Yield: 59 mg (74%). $C_{60}H_{58}Ni_3P_4O_4S_4$ (1271.35): calcd. C 56.68, H 4.60; found C 56.41, H 4.48.

Crystallography: Data were collected at –80 °C with a Siemens Platform/CCD automated diffractometer. Data processing was performed with SAINT PLUS version 6.22. Structures were solved by direct methods and refined using full-matrix least squares on F^2 using Bruker SHELXTL version 6.10. Methyl, carboxyl, and amide H atom thermal parameters were assigned as 1.5× those of the adjacent atom. Remaining hydrogen atoms were fixed in idealized positions with thermal parameters 1.2× those of the attached carbon atoms. CCDC-613254 [Fe_2(aspH)$(CO)_6$], -613255 {Fe_2[$(SCH_2)_2$CHCONHEt]$(CO)_6$}, -613256 {Fe_2[$(SCH_2)_2$-CHCONHCH$_2$CO$_2$*t*Bu]$(CO)_6$}, -613252 [Ni(aspH)(dppe)], and -613253 [$Ni_3(asp)_2(dppe)_2$] contain the supplementary crystallographic data for this paper. These data can be obtained free of charge from The Cambridge Crystallographic Data Centre via www.ccdc.cam.ac.uk/data_request/cif.

Acknowledgments

P. I. V. thanks Dr. Danica P. Galonic for helpful discussions. This research was supported by the National Institutes of Health.

[1] H. Yanagawa, T. Kato, Y. Kitahara, N. Takahashi, Y. Kato, *Tetrahedron Lett.* **1972**, *13*, 2549–2552.
[2] Y. Tsuneo, S. Kikuo (Sumitomo Chemical Co., Ltd., Japan), *Jpn. Kokai Tokkyo Koho* **1985**, JP60011494U.
[3] H. Yanagawa, T. Kato, H. Sagami, Y. Kitahara, *Synthesis* **1973**, 607–608.
[4] R. Singh, G. M. Whitesides, *J. Am. Chem. Soc.* **1990**, *112*, 1190–1197.
[5] Y. Nicolet, A. L. de Lacey, X. Vernède, V. M. Fernandez, E. C. Hatchikian, J. C. Fontecilla-Camps, *J. Am. Chem. Soc.* **2001**, *123*, 1596–1601.
[6] Y. Nicolet, B. J. Lemon, J. C. Fontecilla-Camps, J. W. Peters, *Trends Biochem. Sci.* **2000**, *25*, 138–143.
[7] Y. Nicolet, C. Piras, P. Legrand, C. E. Hatchikian, J. C. Fontecilla-Camps, *Structure* **1999**, *7*, 13–23.
[8] F. Gloaguen, J. D. Lawrence, T. B. Rauchfuss, *J. Am. Chem. Soc.* **2001**, *123*, 9476–9477.
[9] F. Gloaguen, J. D. Lawrence, M. Schmidt, S. R. Wilson, T. B. Rauchfuss, *J. Am. Chem. Soc.* **2001**, *123*, 12518–12527.
[10] Y. Shvo, E. Hazum, *J. Chem. Soc., Chem. Commun.* **1975**, 829–830.
[11] X. Zhao, I. P. Georgakaki, M. L. Miller, J. C. Yarbrough, M. Y. Darensbourg, *J. Am. Chem. Soc.* **2001**, *123*, 9710–9711.
[12] D. Chong, I. P. Georgakaki, R. Mejia-Rodriguez, J. Sanabria-Chinchilla, M. P. Soriaga, M. Y. Darensbourg, *Dalton Trans.* **2003**, 4158–4163.
[13] F. Gloaguen, J. D. Lawrence, T. B. Rauchfuss, M. Benard, M.-M. Rohmer, *Inorg. Chem.* **2002**, *41*, 6573–6582.
[14] T. B. Rauchfuss, D. M. Roundhill, *J. Am. Chem. Soc.* **1975**, *97*, 3386–3392.
[15] Q. Wang, A. C. Marr, A. J. Blake, C. Wilson, M. Schroeder, *Chem. Commun.* **2003**, 2776–2777.
[16] S. S. Oster, R. J. Lachicotte, W. D. Jones, *Inorg. Chim. Acta* **2002**, *330*, 118–127.
[17] P. V. Rao, S. Bhaduri, J. Jiang, D. Hong, R. H. Holm, *J. Am. Chem. Soc.* **2005**, *127*, 1933–1945.
[18] J. A. W. Verhagen, M. Beretta, A. L. Spek, E. Bouwman, *Inorg. Chim. Acta* **2004**, *357*, 2687–2693.
[19] D. M. Roundhill, *Inorg. Chem.* **1980**, *19*, 557–560.
[20] K. Issleib, D. Wienbeck, *Z. Anorg. Allg. Chem.* **1978**, *440*, 5–21.
[21] M. Razavet, S. J. Borg, S. J. George, S. P. Best, S. A. Fairhurst, C. J. Pickett, *Chem. Commun.* **2002**, 700–701.
[22] X. Zhao, Y.-M. Hsiao, C.-H. Lai, J. H. Reibenspies, M. Y. Darensbourg, *Inorg. Chem.* **2002**, *41*, 699–708.
[23] J. D. Lawrence, H. Li, T. B. Rauchfuss, *Chem. Commun.* **2001**, 1482–1483.

Received: July 6, 2006
Published Online: October 19, 2006

